# MACRO-ELEMENT APPROACH FOR TOPOLOGY OPTIMIZATION OF TRUSSES USING A GROUND STRUCTURE METHOD

BY

XIAOJIA(SHELLY) ZHANG

THESIS

Submitted in partial fulfillment of the requirements
for the degree of Master of Science in Civil Engineering
in the Graduate College of the
University of Illinois at Urbana-Champaign, 2014

Urbana, Illinois

Adviser:

Professor Glaucio H. Paulino

# Abstract

In this thesis, the generation of initial ground structures for generic domains in two and three dimensions are discussed. Two methods of discretization are compared: Voronoi-based discretizations and structured quadrilateral discretizations. In addition, a simple and effective member generation approach is proposed: the Macro-element approach; which can be implemented with both types of discretization. The features of the approach are discussed: efficient generation of initial ground structures; reduction in matrix bandwidth for global stiffness matrix; finer control of bar connectivity; and reduction of overlapped bars. Numerical examples are presented which display the features of the proposed approach, and highlight the comparison with literature results and traditional ground structure generation methods.

*To my mother, Yanhua and my father, Jiguo.*

# Acknowledgements

First and foremost, I would like to express my deepest gratitude to my advisor, Professor Glaucio H. Paulino, without whom this work would not have been possible. His tremendous energy about research, constant support and encouragement have had a profound impact on my professional life.

Sincere thanks are due to Professor Gholamreza Mesri, who helped me tremendously during my undergraduate and graduate years, every discussion with him was inspiring. This thesis would not have been possible without the contribution of Professor Adeildo Soares Ramos Jr. whose guidance and suggestions were instrumental in this work.

I would also like to thank all of my colleagues, Cameron Talischi, Lauren Beghini, Arun Gain, Tomas Zegard, Sofia Leon, Daniel Spring, Junho Chun, Evgueni Filipov, Heng Chi, Maryam Eidini, Tuo Zhao, Ke Liu, Ludimar Lima de Aguiar, Adeildo Soares Ramos Jr., Luis Arnaldo, Peng Wei for their help and support. I own my special gratitude to Sofia Leon and Tomas Zegard, for donating their time giving me invaluable helps during my graduate life; Heng Chi, for many fruitful discussions and suggestions during my graduate study; Cameron Talischi, for all the inspiration during each discussion; and Daniel Spring, for helping me polish and proof read this thesis.

Additionally, I also thank my friends: Aobai Wang, Chen Ma, Xiao Ma for their continued support and encouragement. I am extremely thankful for the camaraderie and kindness they have provided throughout this time.

Finally, I wish to thank my parents, for their unconditional love and support. No words can describe my appreciation for everything they have done for me. It is with great pleasure that I dedicate this thesis to them.

# Table of Contents

# LIST OF FIGURES

# LIST OF TABLES

# Nomenclature

| | |
|---|---|
| $\boldsymbol{a}$ | Cross-sectional areas vector |
| $a_i^{\max}$ | Maximum area for member $i$ |
| $a_i^{\min}$ | Minimum area for member $i$ |
| $a_o$ | Average area |
| $\boldsymbol{b_i}$ | Geometry vector of member $i$ |
| $C(\boldsymbol{a})$ | Objective function |
| $E_i$ | Young's Modulus for member $i$ |
| $\boldsymbol{f}$ | External force vector |
| $g(\boldsymbol{a})$ | Constraint function |
| $\boldsymbol{K}$ | Global stiffness matrix |
| $\boldsymbol{K_i^0}$ | Constant element stiffness matrix |
| $\boldsymbol{L}$ | Member's length vector |
| $\ell_i$ | Length for member $i$ |
| $M$ | Number of bars |
| $move$ | Move limit |
| $N$ | Number of nodes |
| $\boldsymbol{n_i}$ | Unit vector in axial direction of the member $i$ |
| $tol$ | Tolerance |
| $\boldsymbol{u}$ | Nodal displacement vector |
| $V_{\max}$ | Maximum material volume |
| $\boldsymbol{y}$ | Intermediate variable vector |
| $q$ | Number of load cases |
| $\alpha_j$ | Weighting factor of load case $j$ |

| | |
|---|---|
| $\boldsymbol{\lambda}$ | Adjoint variable |
| $\phi$, $\beta$ | Lagrange multipliers |
| $\Psi_i$ | Potential energy of the member $i$ |
| $\eta$ | Numerical damping factor in OC |

# List of Abbreviations

| | |
|---|---|
| 2D | Two-Dimensional |
| 3D | Three-Dimensional |
| FEM | Finite Element Method |
| GSM | Ground Structure Method |
| KKT | Karush-Kuhn-Tucker |
| OC | Optimality Criteria |

# Chapter 1

# Introduction

## 1.1 Motivation

The ground structure method (GSM) [2, 3, 4] , is a technique for truss layout optimization. The generation of the initial ground structure, as a crucial component of the ground structure method, has so far received little attention in literature. Smith [5] proposed an approach for the generation of ground structures, using unstructured meshes to represent the design domain. However, the approach he proposes requires additional preprocessing steps; including the decomposition of design elements and the generation of boundary faces. In this thesis, a simple and effective approach is proposed for generation of ground structures, namely the Macro-element approach. This approach is capable of generating ground structures for design domains of non-trivial geometries with ease, and does not require any additional information on the outer and inner boundaries of the domain. This approach is proposed in a general setting – it may be combined with any type of discretization, including quadrilateral and Voronoi-based elements in two or three dimensional domains. The elastic formulation is adopted in this thesis [3].

One limitation associated with the traditional GSM is that, for concave domains $\Omega$, as illustrated in Figure 1.1(a), or for separated design domains, $\Omega_1$ and $\Omega_2$, as illustrated in Figure 1.1(b); one needs to verify that connections don't fall outside the boundary (for concave domains), or cross the border of separated design domains. With the approach presented in this thesis, these problems are naturally avoided.

## 1.2 Background on Ground Structure Method

In GSM, the structural domain is first discretized by nodes, and then the nodes are connected by the truss members. For a full-level ground structure,

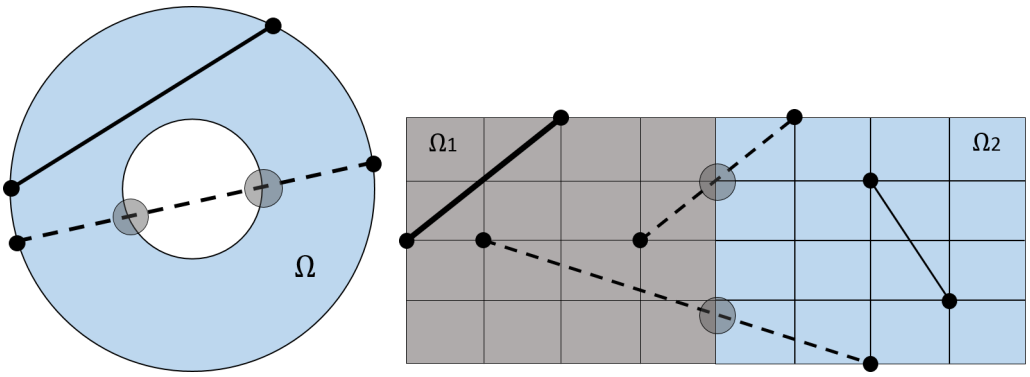


(a) (b)

Figure 1.1: Optimization problems using traditional GSM with solid lines for allowed connections and dashed lines for violated connections: (a) concave domain; (b) convex domain with separated design regions.

all nodes in the domain are connected to one another. This leads to a fully populated global stiffness matrix, which adds to the computational cost [6]. Alternatively, definitions of different connectivity levels have been described in the literature [7]. The basic idea behinds the different levels is that, in general, long bars are not needed in the ground structure. Thus, many bars in full-leveled ground structures are unused in the optimization process [8]. In addition, lower levels of connectivity may reduce the computational cost associated with these unused bars in the optimization. However, one problem with the leveling method is that the assignment of a sufficient connectivity level is problem dependent, making it impractical to define a general ground structure level for all problems. Different connectivity levels can result in different topologies for the same problem, as illustrated in Figure 1.2, Figure 1.3 and Figure 1.4: final topology from level 2 ground structure in Figure 1.3(b) has the fewest number of bars, while topology from full level in Figure 1.4(b) provides the best solution in terms of compliance. In the current work, only full level ground structures are considered in classic GSM.

Overlapping bars are undesirable in the GSM and can be addressed during the generation process. Alternatively, the overlapping members can be removed after the generation process is complete. Figure 1.5 shows a simple example which highlights the importance of removing overlapping bars. The solution of this problem is trivial: one straight horizontal member carries all the load to the supports. When overlapping bars are not removed, the member sizes are not equal, as can be seen in Figure 1.5(d) (solution is not

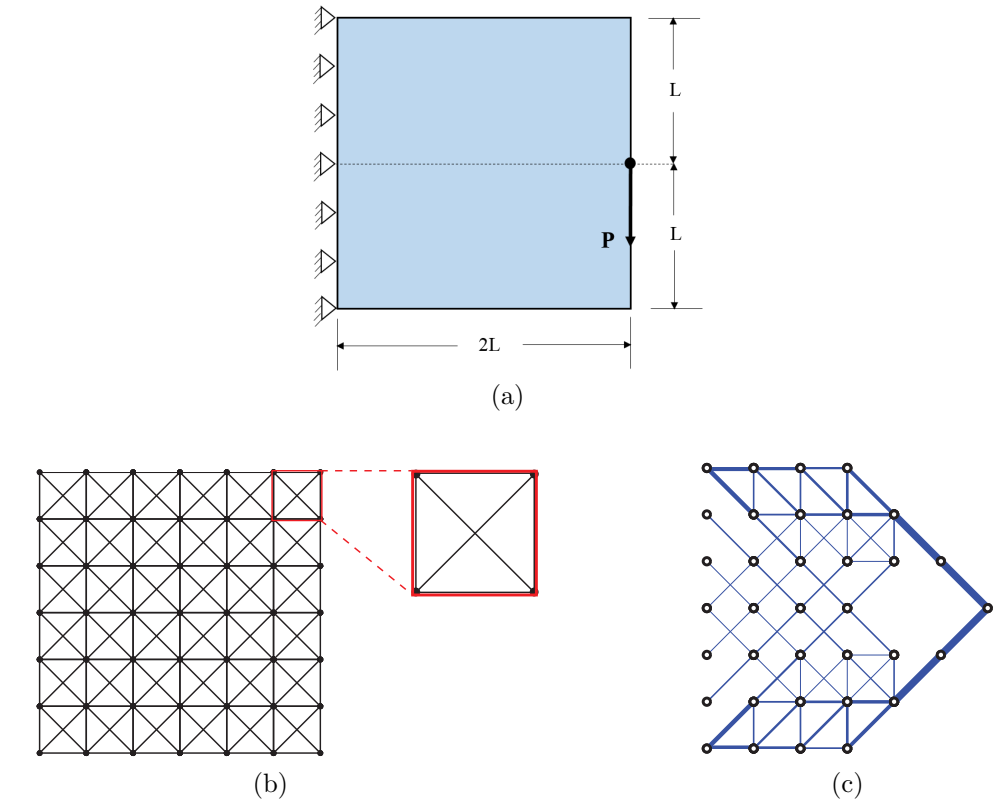


Figure 1.2: Generation of ground structure for level 1 connectivity: (a) problem domain and boundary conditions; (b) initial ground structure; (c) optimal topology.

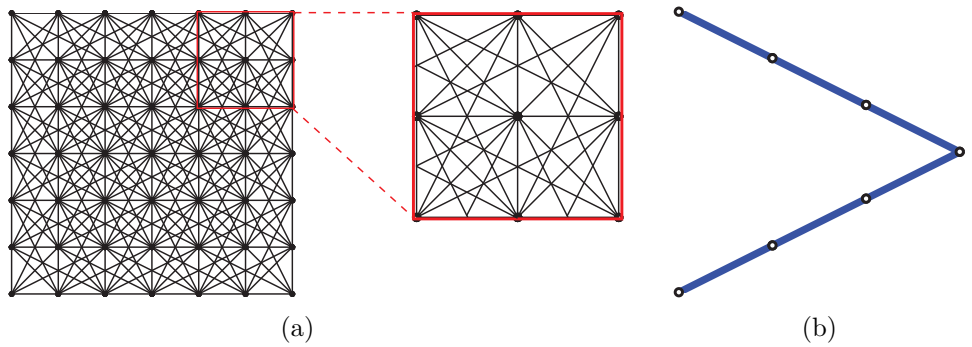


Figure 1.3: Generation of ground structure for level 2 connectivity: (a) initial ground structure; (b) optimal topology.

(a) (b)

Figure 1.4: Generation of ground structure for full level connectivity: (a) initial ground structure; (b) optimal topology.

unique). However, when overlapping bars are removed, all member sizes are equal, as shown in Figure 1.5(e). Thus, it is important to remove overlapping members in order to obtain meaningful results in even the simplest examples. In addition, this lowers the total number of bars in the model and decreases the computational cost of the method. In the present work, overlapping bars are removed during the bar generation process.

Michell [1] derived analytical solutions for many interesting optimization problems. He showed that, for a structure to be optimal, all members should be fully stressed. This leads to the requirement that all tensile and compressive bar pairs should intersect each other orthogonally (for problems without material or geometric non-linearities). Therefore, if we assume all bars to have the same stress limits, the orthogonality in pairs of bars should appear in the optimal solutions[9]. Figure 1.6(a) shows an optimization problem for a simply supported beam with its discrete Michell's solution shown in Figure 1.6(b). Michell's solution is actually continuous solution (infinitely dense members), when using the traditional GSM, the Michell's solution can be approximated by a very fine initial ground structure. However, this comes with a high computational cost. In Chapter 3, the optimization problem in Figure 1.6(a) is investigated with highly refined ground structures using both the traditional GSM and the proposed approach.

## 1.3 Thesis Organization

The thesis is organized as follows: in Chapter 2, the ground structure optimization formulation is reviewed for compliance minimization using only the

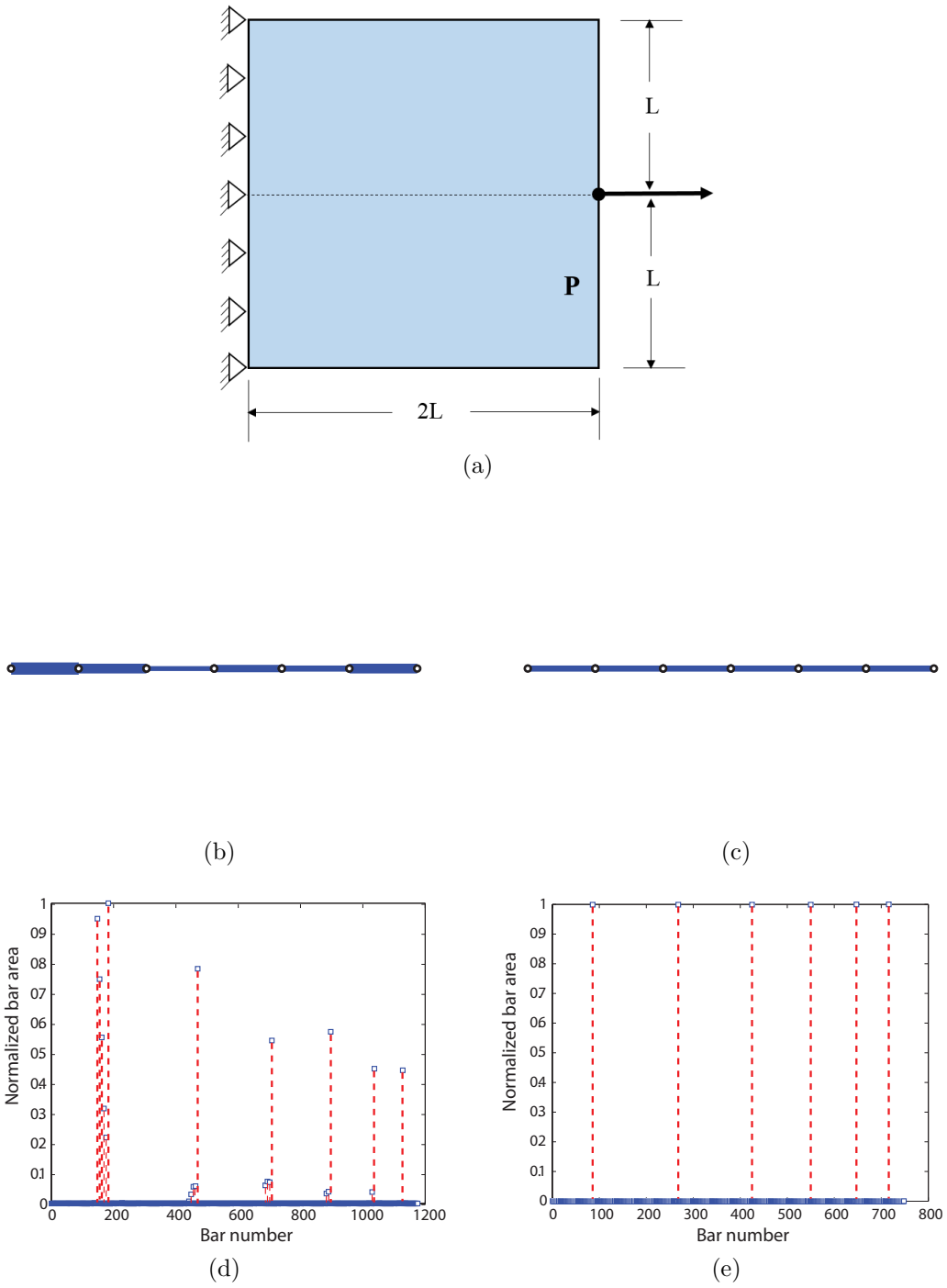


Figure 1.5: Topology optimization with and without overlapping bars in a box domain: (a) problem domain and boundary conditions; (b) optimal topology with overlapping connections; (c) optimal topology with non-overlapping connections; (d) bar areas distribution with overlapping bars; (e) bar areas distribution with non-overlapping bars.

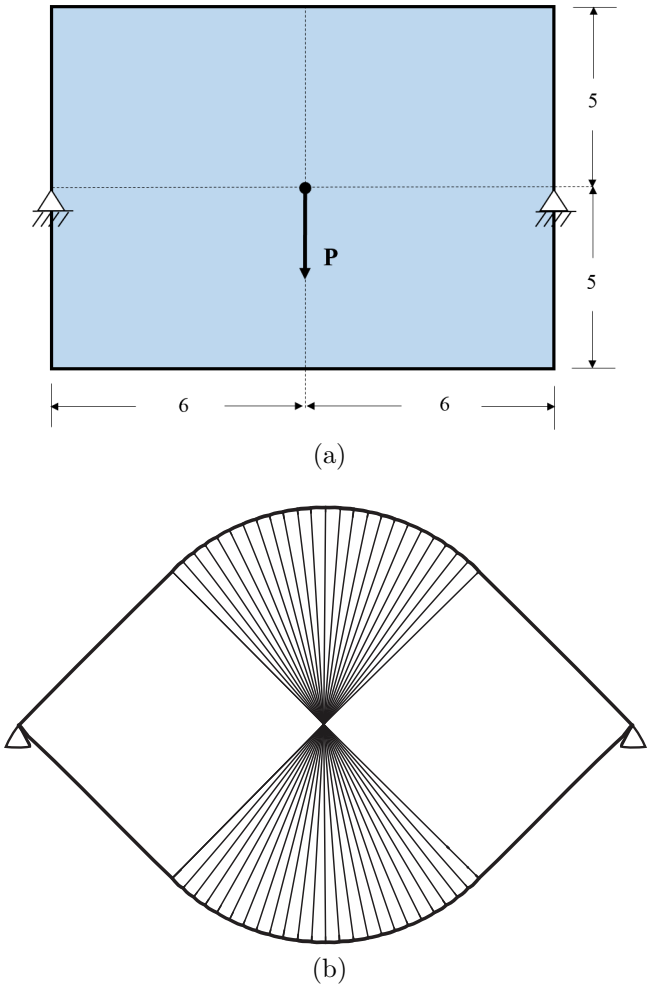


Figure 1.6: Michell's solution in a box domain: (a) domain with boundary conditions; (b) known analytical solution [1].

cross-sectional areas of the bars as the design variables. Then, discretization methods and the proposed approach are introduced in Chapter 3, namely the Macro-element Approach, which are used in the generation of initial ground structures, and followed by a discussion of its attributes for optimization of trusses using the Ground Structure Method. Several numerical examples are presented in Chapter 4 to highlight the properties of the new approach. Finally, summary and conclusion are given with suggestions of the extension of this work in the future.

# Chapter 2

# Problem Formulation

## 2.1 Optimization Formulation

The formulation used in the present work considers equilibrium and compatibility conditions, which explicitly is known as elastic analysis [10]. The initial ground structure is given with $N$ nodes and $M$ members. The equilibrium state of the system can be described by:

$$\boldsymbol{K}\boldsymbol{u} = \boldsymbol{f} \tag{2.1}$$

where, for the case of a two-dimensional problem, $\boldsymbol{f} \in R^{2N}$ is the external force vector, $\boldsymbol{u} \in R^{2N}$ is the displacement vector and $\boldsymbol{K} \in R^{2N*2N}$ is the stiffness matrix. For a full level ground structure in a convex domain, before removing overlapping bars, the relation between $M$ and $N$ is $M = \frac{N(N-1)}{2}$.

The stiffness matrix K may be expressed as [3]:

$$\boldsymbol{K}(\boldsymbol{a}) = \sum_{i=1}^{M} a_i \boldsymbol{K}_i^0, \qquad \boldsymbol{K}_i^0 = \frac{E_i}{\ell_i} \boldsymbol{b_i} \boldsymbol{b_i^T} \tag{2.2}$$

where $\boldsymbol{K}_i^0$ is a constant matrix associated to each member in global coordinates, $E_i$ and $\ell_i$ are Young's Modulus and length of member $i$, respectively. Moreover, $\boldsymbol{a} \in R^M$ is a vector of design variables (areas of bars) for the optimization problem, and $\boldsymbol{b_i}$ is a vector describing the direction in the orientation of member i with the form:

$$\boldsymbol{b_i} = \begin{Bmatrix} \vdots \\ -\boldsymbol{n}^{(i)} \\ \vdots \\ \boldsymbol{n}^{(i)} \\ \vdots \end{Bmatrix} \tag{2.3}$$

where $\boldsymbol{n}^{(i)}$ is a unit vector in the axial direction of the member $i$.

Here, the optimization problem is defined as one which finds the set of design variables that minimizes compliance of the structure, subject to equilibrium and volume constraints. Because the main purpose of this thesis is to explore the connectivity generation in the ground structure, the simplest displacement based formulation is adopted, with a small positive lower bound imposed on the design variables $a_i$. In that case, the stiffness $\boldsymbol{K}$ will be positive definite for the whole feasible set of design variables. The convexity of the problem can also be shown and the existence of solution is guaranteed [11]. The problem statement with multiple load cases can be formulated as [4]:

$$C(\boldsymbol{a}) = \min_{\boldsymbol{a}} \sum_{j=1}^{q} \alpha_j \, \boldsymbol{f}_j^T \, \boldsymbol{u}_j(\boldsymbol{a})$$

$$\text{s.t.} \begin{cases} g(\boldsymbol{a}) = \boldsymbol{a}^T \boldsymbol{L} - V_{\max} \leq 0 \\ \\ a_i^{\min} \leq a_i \leq a_i^{max} \quad \forall \, i = 1 \, : \, M \end{cases} \tag{2.4}$$

where $\boldsymbol{u}_j$ is the solution of Equation (2.1), $C(\boldsymbol{a})$ is the objective function, $q$ is the number of load cases, $\alpha_j$ is the weighting factor of load case $j$, $g(a)$ is the constraint function, $\boldsymbol{a}$ and $\boldsymbol{L}$ are the vectors of area and length, respectively, $V_{\max}$ is the maximum material volume, and $a_i^{max}$ and $a_i^{\min}$ are the upper and lower bounds, respectively.

This formulation allows computing the element stiffness matrices only once. The global stiffness matrix can then be assembled from the element stiffness matrices and current design variables (member cross-sectional areas). This facilitates a more efficient implementation. To avoid a singular tangent stiffness matrix in the solution of the structural linear equation (2.1), we prevent zero element areas by using a small lower bound, $a_i^{\min}$. The upper and lower bounds are defined by $a_i^{max} = 10^3 a_0$ and $a_i^{\min} = 10^{-2} a_0$, respectively; where $a_0$ is the average area.

$$a_0 = \frac{V_{\max}}{\sum_i L_i} \tag{2.5}$$

## 2.2 Implementation Aspects

The concepts in this thesis have been implemented in a complete truss layout optimization solver in MATLAB ®. The implementation consists of two components: ground structure generation and optimization. The ground structure generation process includes base mesh generation and connectivity generation. Three alternatives for generating the base mesh for the domain geometry are employed: generating a Voronoi-based mesh using the mesh generator for polygonal elements named PolyMesher [12], generating a structured quadrilateral mesh using an intrinsic subroutine, or importing an unstructured mesh from elsewhere. Here, the main idea of the ground structure generation is to produce non-overlapping connectivity using the base mesh. The testing for mutual overlapped connections is an additional procedure for the connectivity generation for the traditional GSM. The optimization process contains three components: solving the structural problem for a set of given design variables, computing the sensitivities of the design variables, and updating the design variables based on the Optimality Criteria (OC). The details of the sensitivity calculations, Karush-Kuhn-Tucker (KKT) conditions and OC are provided in the appendices.

# Chapter 3

# Ground Structure Generation

## 3.1 Base Mesh

In this work, two types of mesh are used to discretize the domain: structured quadrilateral mesh and Voronoi-based mesh, as shown in Figure 3.1. The need for different types of mesh is problem dependent.

A full level ground structure, using a structured quadrilateral mesh, provides pairs of orthogonal bars by construction, but they tend to be oriented in a limited number of directions. In addition, when the domain is complex, this meshing procedure is generally tedious and complicated. Because the stiffness matrix is densely populated in the case of the full level GSM, the associated computational cost is quite high [6].

Based on these issues, the use of the Voronoi-based mesh is proposed. Voronoi-based meshes easily discretize non-convex domains and have been shown to be advantageous in continuum topology optimization [13, 12]. The seeds of Voronoi-based meshes are initially generated randomly, then iterated to align uniformly using the Centroid Voronoi Tessellation (CVT) method. After extracting node and element information, the optimization procedure is the same as with structured quadrilateral meshes. Voronoi-based meshes, as opposed to structured quadrilateral meshes, can generate bars with a greater number of directions, because of its random node distribution, but provides fewer orthogonal pairs of bars; which is not desirable according to the Michell's solution [1].

When the domain is concave or contains holes, the Voronoi-based grid is the preferred discretization in this work. However, for these domains, generating a full level, non-overlapping initial ground structure, is complicated. As the generated bars have to lie entirely within the domain, not all connections are feasible. Therefore, additional information on the outer and inner boundaries of the domain is needed with respect to the traditional GSM.

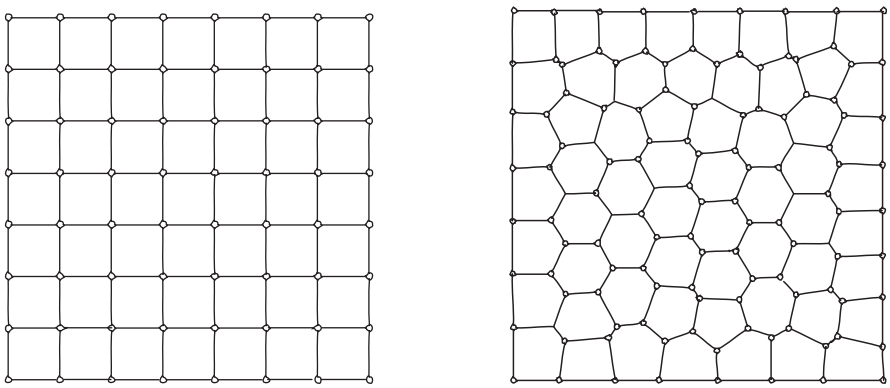

(a) (b)

Figure 3.1: Discretization techniques for forming the base mesh: (a) structured quadrilateral mesh; (b) Voronoi-based mesh.

This issue is naturally solved by the member generation approach that is proposed, which is further discussed in Section 3.2.2.

## 3.2 Member Generation Approach

In this section, a new approach for generating initial ground structures using structured quadrilateral and Voronoi-based meshes in two or three-dimensional domains is presented. A Macro-element approach is proposed to overcome some of the difficulties in ground structure generation, as discussed above. The resulting generation of the ground structure, using this technique, is almost fully automated and efficient.

### 3.2.1 Macro-element Approach

The basic idea behind this method is to insert equally spaced nodes on each edge of each element, then connections are only generated within each element. An illustration of the Macro-element approach using a structured quadrilateral mesh and a Voronoi-based mesh is shown in Figure 3.2, Figure 3.3, Figure 3.4 and Figure 3.5. Different scenarios were considered, to show the flexibility of this method: four equally spaced nodes were inserted on each edge for the structured quadrilateral mesh in Figure 3.2 and Figure 3.3; three additional nodes were inserted per edge for the single Voronoi-based mesh in Figure 3.4; and one node was inserted per edge for the quarter ring domain example. This method can also be used in three dimensional (3D)

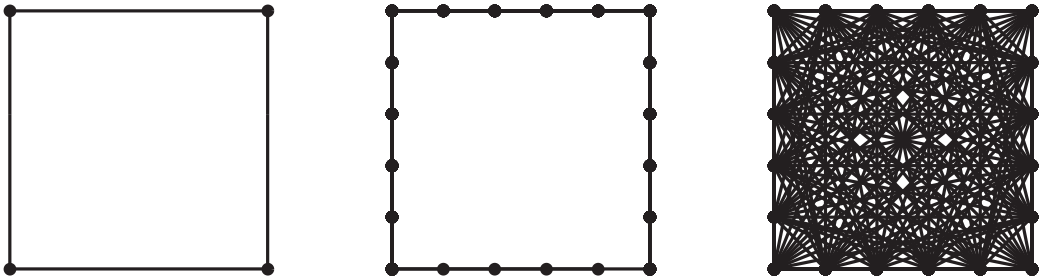

(a) (b) (c)

Figure 3.2: Macro-element approach using a structured quadrilateral element with 4 nodes inserted per edge: (a) single structured quadrilateral element; (b) single element with inserted additional nodes on each edge; (c) all possible connections within the element.

domains, as shown in Figure 3.6.

### 3.2.2 Attributes and Properties

The properties of the Macro-element approach relate to the ground structure generation process, optimization process and final topology aspect. In the ground structure generation process, the proposed approach avoid invalid connections outside the boundary (for concave domains) by construction, as illustrated in Figure 3.7(a). This can also be used to prevent connections across separated design domains, $\Omega_1$ and $\Omega_2$ as in Figure 3.7(b). Therefore, the bars can be generated without the additional step of detecting boundaries or checking for feasible connections. For the case of concave domains, the initial ground structure can be generated efficiently as long as the domain is discretized and the element connectivity matrix is known. This approach is efficient in terms of the initial ground structure generation.

Another aspect of the approach is in the optimization process. The global stiffness matrix using the two new approach will have a reduced matrix bandwidth. This advantage becomes important when the problem size is large. After nodes are inserted in the edge of each element, the Reverse Cuthill–McKee (RCM) algorithm [14] is used to renumber the nodes. Since bars are only generated in each element, the bandwidth for the global stiffness matrix of the problem will be reduced accordingly.

In terms of final topology, the Macro-element approach offers more control in the bar distribution by providing a finer control of the connectivity.

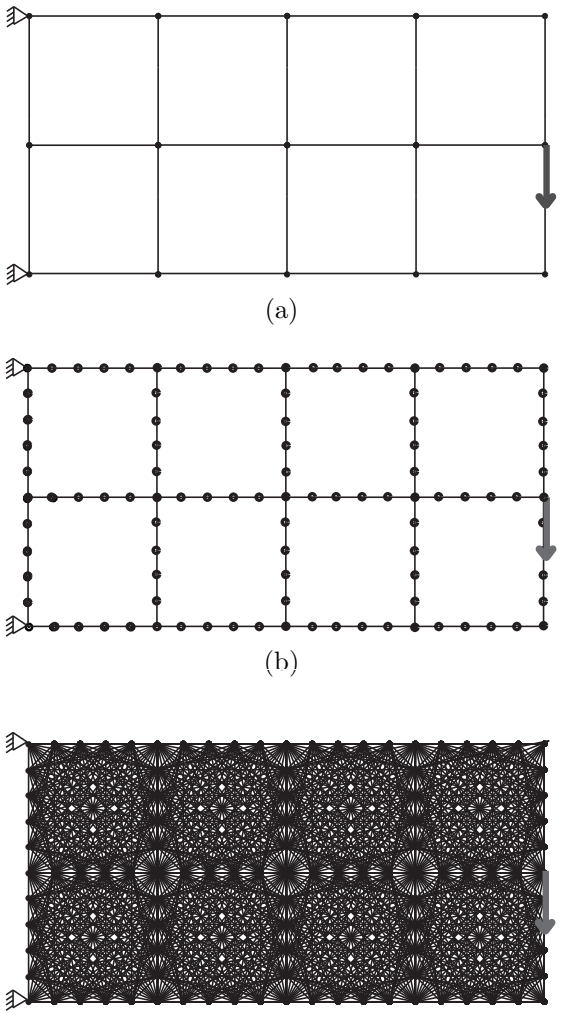

Figure 3.3: Macro-element approach using a structured quadrilateral mesh with 4 nodes inserted per edge: (a) box domain discretized into 8 elements and boundary conditions; (b) box domain with 4 nodes inserted on each edge; (c) all possible connections within each element.

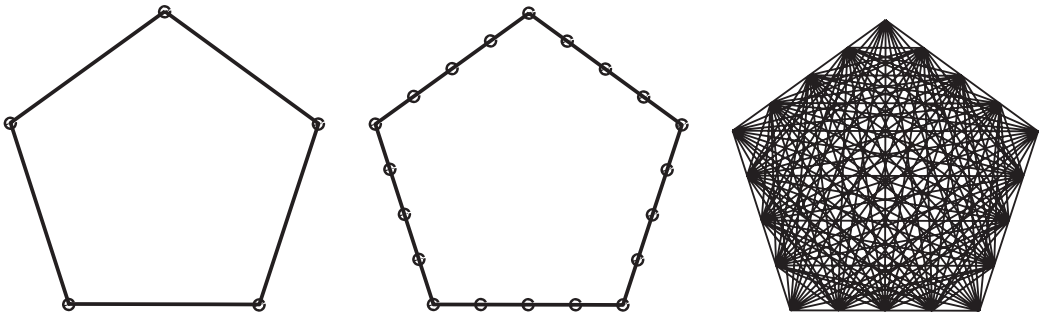

(a) (b) (c)

Figure 3.4: Macro-element approach using Voronoi-based element with 4 nodes inserted per edge: (a) single Voronoi-based element; (b) single element with inserted additional nodes on each edge; (c) all possible connections within the element.

Whether a long straight bar is desired or a curved bar is needed between two nodes, the proposed approach can be used to obtain the desired connectivity, as illustrated in Figure 3.8(b). The standard GSM, on the other hand, either has limited connections or very dense ground structures.

Furthermore, the proposed method does not generate overlapping bars in the domain. For the Macro-element approach, overlapping bars appear only in the (refined) element boundary, and can be efficiently and systematically removed. Therefore, the problem of finding and removing these bars becomes a reduced local problem with an associated lower computational cost.

The proposed approach is general enough to be used with any type of elements, including quadrilateral elements and Voronoi-based elements. This technique can handle different types of domains, concave or convex and in two or three-dimensions. Also, since the Macro-element approach is independent from the optimization formulations, it is flexible and can be extended to other applications with ease.

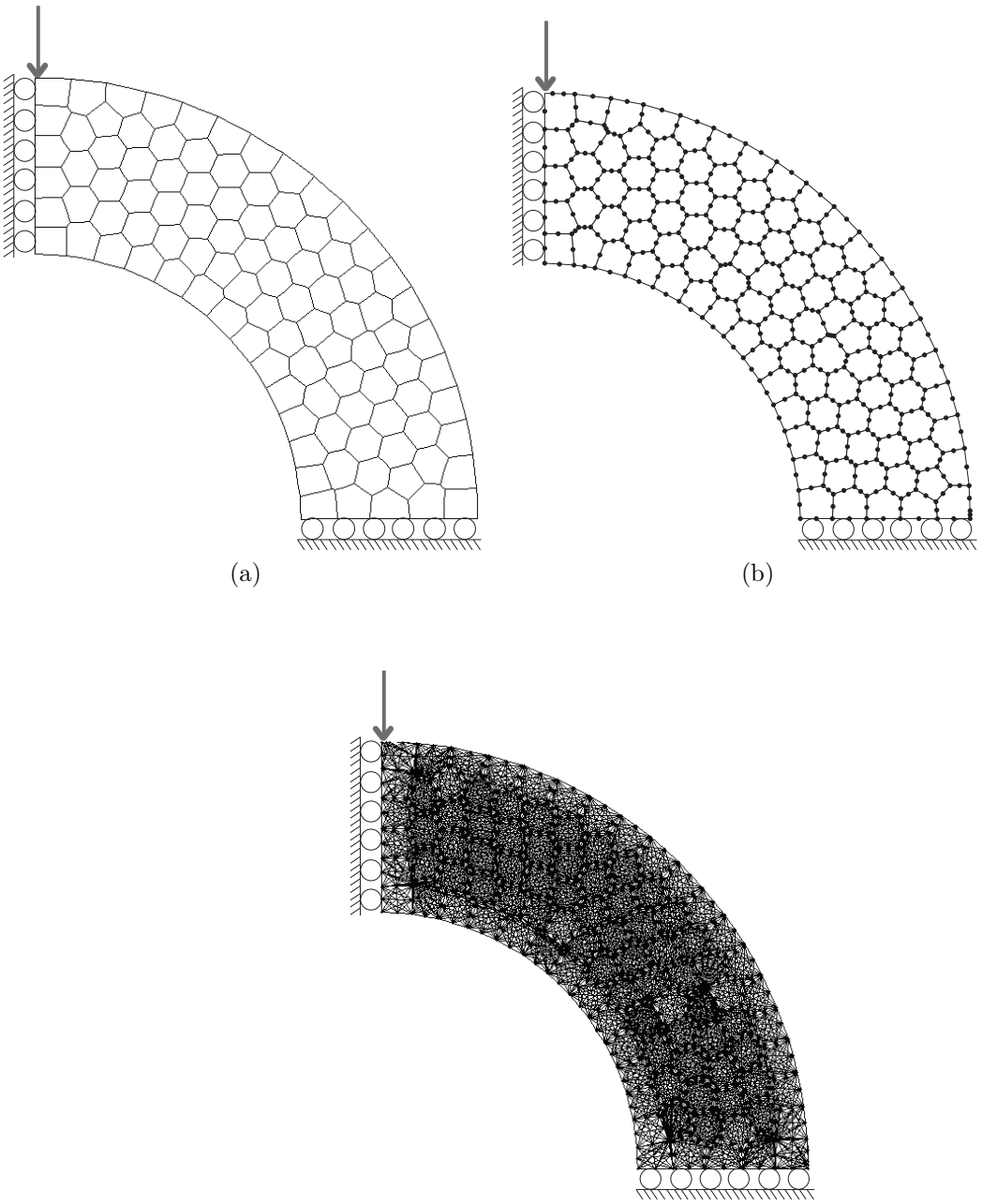

Figure 3.5: Macro-element approach using Voronoi-based mesh with 4 nodes inserted per edge: (a) half ring domain and boundary conditions; (b) half ring domain with 1 node inserted on each edge; (c) all possible connections within each element.

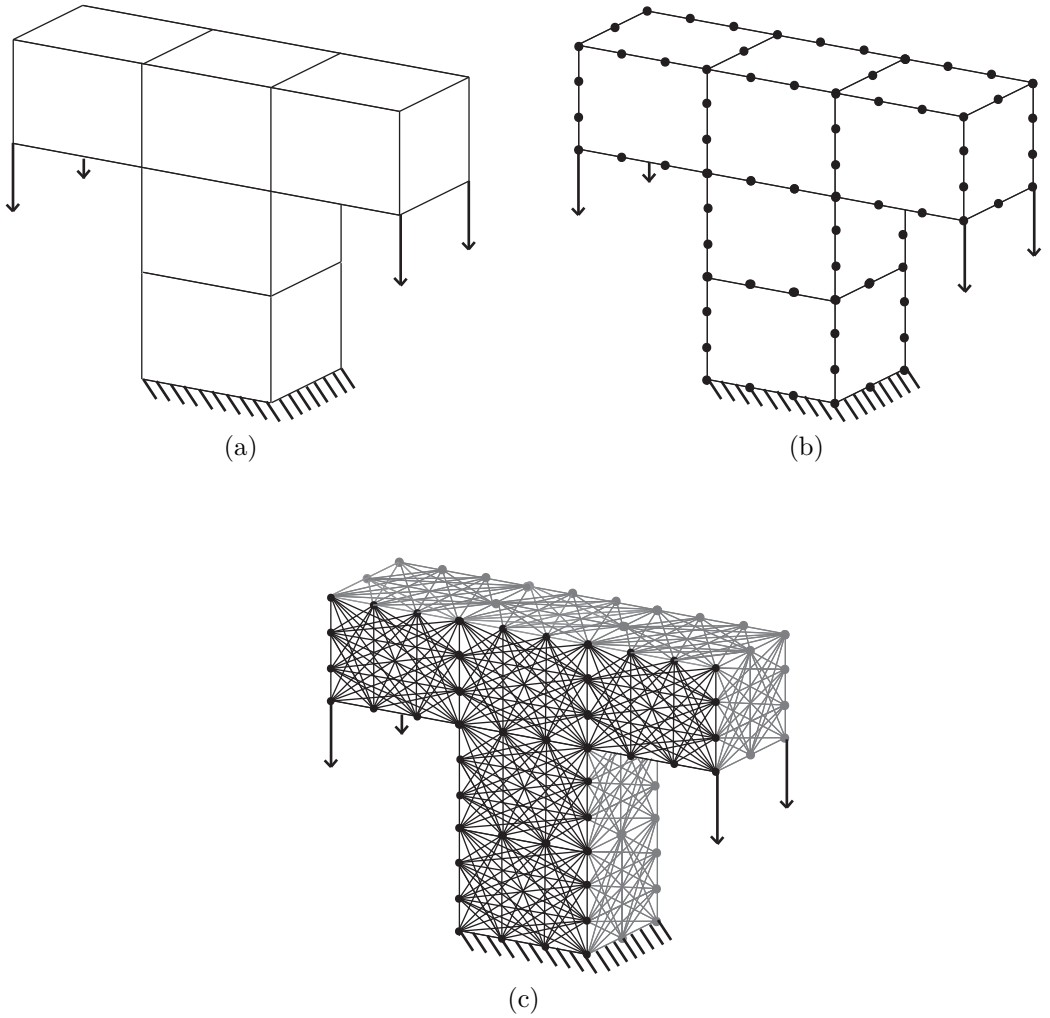


Figure 3.6: Macro-element approach using structured quadrilateral mesh in 3D tower domain: (a) tower domain and boundary conditions; (b) 2 nodes inserted on front surface edges and 1 node inserted on side surface edges; (c) all possible connections within each element surface.

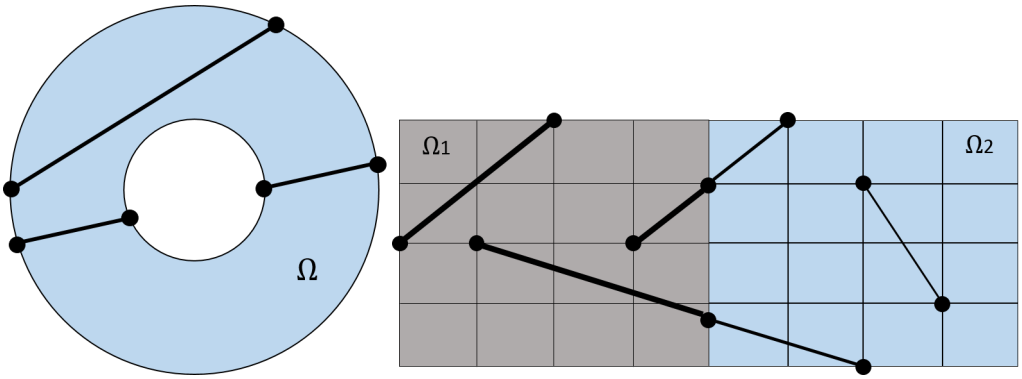


(a) (b)

Figure 3.7: Optimization problems using Macro-element approach to correctly generate initial ground structures with valid connections: (a) concave domain; (b) convex domain with separated design domains.

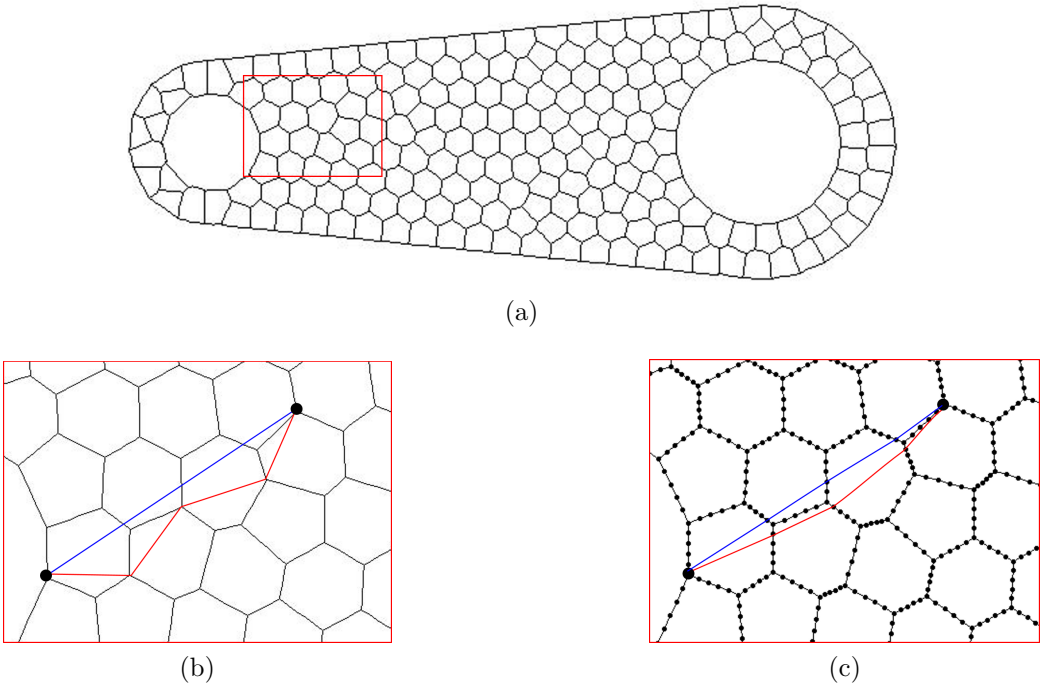

(a)

(b) (c)

Figure 3.8: (a) Wrench domain with a boxed zoom-in region; (b) possible connections using the classic GSM; (c) possible connections using the Macro-element approach.

# Chapter 4

# Examples and Verifications

In this section, three examples will be presented to demonstrate the various features of the proposed approach. All examples are investigated using the same volume constraint: $V_{\max} = A_\Omega * t$, where $A_\Omega$ is the area of the domain; stopping criteria: $tol = 10^{-8}$; move value: $move = (a_i^{\max} - a_i^{\min}) * 100$ and damping factor for the OC update scheme: $\eta = 0.7$. The Young's modulus for all the bars is taken to be $E_0 = 2 \times 10^8$ and the initial guess of bar areas is chosen as: $a_{\text{initial}} = 0.7 * a_0$. The three examples use the Macro-element approach with Voronoi-based elements and quadrilateral elements, and include a comparison with the traditional GSM.

## 4.1 Macro-Element Approach: Comparison with Analytical Solution

In this example, the main idea is to are both the traditional GSM and the Macro-element approach to approximate the Michell's solution shown in Figure 1.6. Both structured quadrilateral and Voronoi-based discretizations are used in solving the box domain with the traditional GSM and the Macro-element approach. Key features of the results are presented in Table 4.1.

The final topologies, using the full level traditional GSM with a dense structured quadrilateral mesh and a Voronoi-based mesh are illustrated in Figure 4.1(a) and Figure 4.1(b), respectively. The final topologies from these dense meshes are similar to the analytical solution shown in Figure 1.6(b), but contain multiple layers along the boundary lines. By using the proposed Macro-element approach, the topologies are very close to the analytical solution, as shown in Figure 4.1(c) and Figure 4.1(d), for the structured quadrilateral and Voronoi-based meshes, respectively. Hence, using the proposed method, we can get a good approximation to the analytical solution.

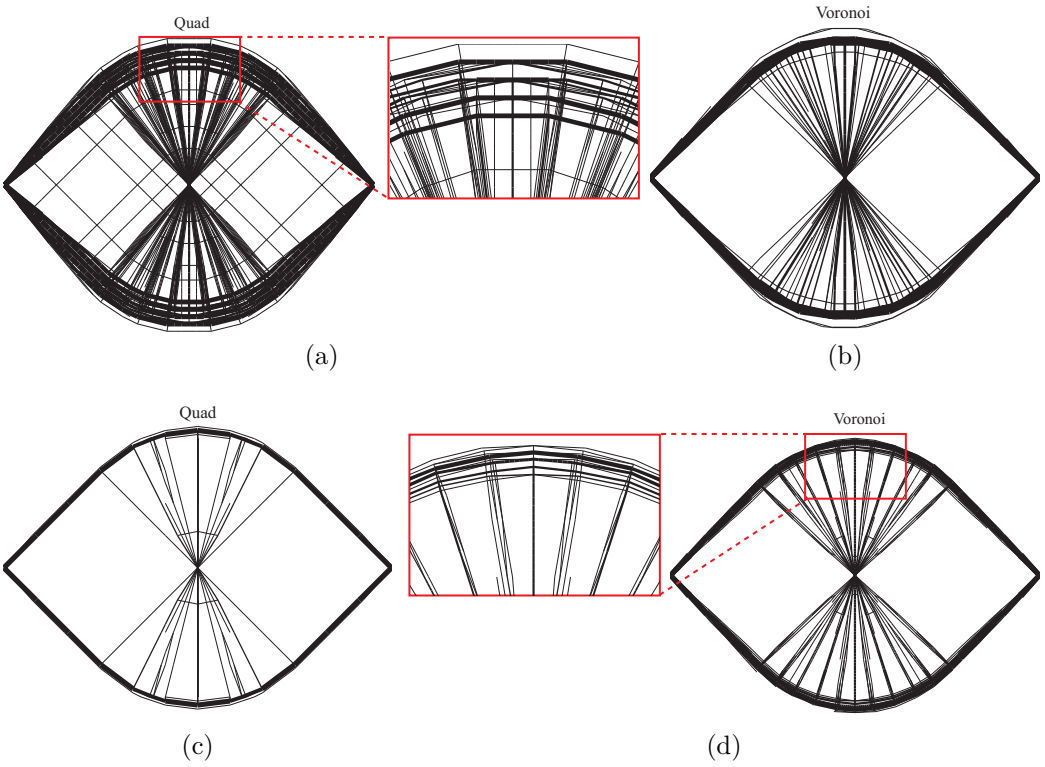


Figure 4.1: Approximation of Michell's solution in a box domain using both structured quadrilateral meshes and Voronoi-based meshes: (a) topology obtained from the traditional GSM with 2000 structured quadrilateral elements; (b) topology obtained from the traditional GSM with 800 Voronoi-based elements; (c) topology obtained from the Macro-element approach using 120 structured quadrilateral elements with 7 nodes inserted along each edge; (d) topology obtained from the Macro-element approach using 240 Voronoi-based elements with 7 nodes inserted along each edge.

| Mesh | GSM | Number of Bars | Compliance |
|---|---|---|---|
| Quadrilateral Mesh (Figure 4.1(a), (c)) | Traditional | 77710 | 1.7205 |
| | Macro-element | 59520 | 1.6800 |
| Voronoi-based Mesh (Figure 4.1(b), (d)) | Traditional | 135280 | 1.7099 |
| | Macro-element | 192272 | 1.7065 |

Table 4.1: Numerical information for Example 4.1.

| GSM | Number of Bars | Compliance Value |
|---|---|---|
| Traditional GSM | 92188 | 0.201 |
| Macro-Element | 215200 | 0.182 |

Table 4.2: Numerical information for wrench domain.

## 4.2 Macro-Element Approach: Applications to Complex Domains

In the second and third examples, we apply the Macro-element approach to both the Wrench and Serpentine domains introduced in Talischi et al. [12]. These are non-trivial domains and showcase the capabilities of this approach for arbitrary domains. Again, the final topologies are compared with those obtained using the traditional GSM.

### 4.2.1 Wrench Domain with Voronoi-based Mesh

The first problem considers the Wrench domain, with a Voronoi-based discretization, as shown in Figure 4.2. The idea is to compare the final topology and the number of bars that both methods produce under similar computational cost. In the traditional GSM, 1000 Voronoi-based elements were used to discretize the domain, as illustrated in Figure 4.2(b). A full level connectivity was generated within the domain. Overlapping bars were removed during the bar generating process. The final topology is shown in Figure 4.2(d). The boundary lines around the right hole in the final topology are not smooth, and the bars in the middle of the domain are not detailed. The base mesh used in the Macro-element approach is shown in Figure 4.2(c); discretized by 260 Voronoi-based elements with 7 additional nodes inserted along each edge. The bars were only connected within each element. The time spent for mesh generation is similar to that for the full-level GSM, and the final topology using the Macro-element approach is shown in Figure 4.2(e). Qualitatively, if we compare the results from the two methods, the Macro-element approach results in a clear and crisp solution around the right hole, and the bars inside the domain are smoother than those obtained using traditional GSM. In addition, the solution obtained using the Macro-element approach exhibits the close-to-orthogonal pairs of bars.

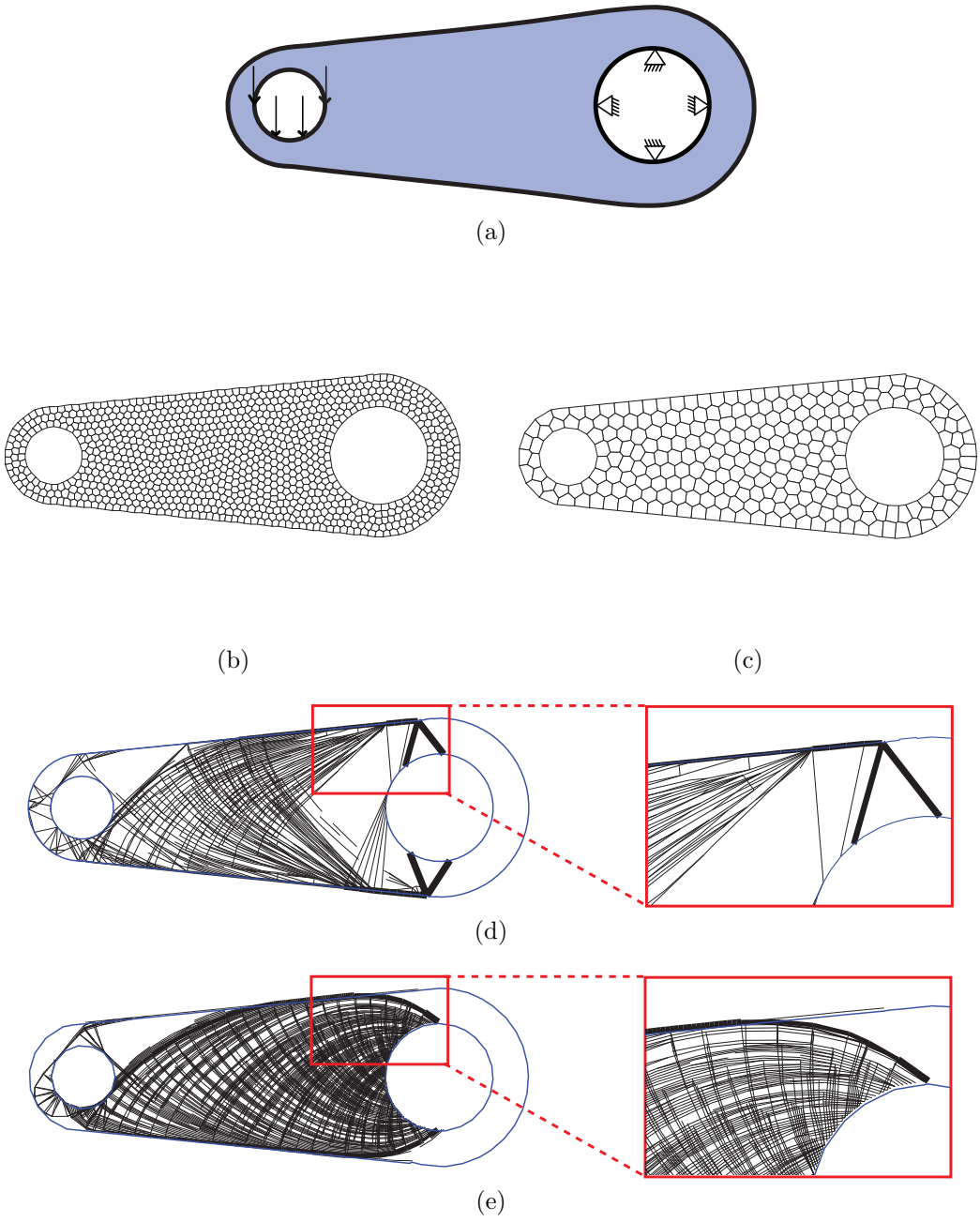


Figure 4.2: Wrench domain example with Voronoi-based mesh using classic GSM and Macro-element approach: (a) wrench domain and boundary conditions; (b) discretization using 1000 Voronoi-based elements; (c) discretization using 260 Voronoi-based elements with 7 additional nodes inserted along each edge; (d) final topology using the full level classic GSM; (e) final topology using the Macro-element approach.

| GSM | Normalized max. semi-bandwidth | Normalized profile |
|---|---|---|
| Full Level | 0.8496 | 0.7729 |
| Macro-element | 0.0556 | 0.0695 |

Table 4.3: Bandwidth and profile comparison of the stiffness matrix for Wrench domain with different bar generation method.

A comparison of the number of bars in the initial ground structures and the final compliance values between the traditional GSM and the Macro-element approach is presented in Table 4.2. This showcases the ability of the Macro-element approach to handle large problems with an associated low computational cost in ground structure generation. For the case of concave domains, the time spent in the bar generation process is greatly reduced in the Macro-element approach, because there is no need to detect the boundary or search for a large number of overlapping bars.

The source of the computational efficiency of the Macro-element approach is apparent when we compare the bandwidth and profile of the stiffness matrix for both methods. The normalized maximum semi-bandwidth and normalized profile are computed as:

$$\text{normalized maximum semibandwidth} = \frac{\text{max.semibandwidth}}{2N} \tag{4.1}$$

$$\text{normalized profile} = \frac{\text{profile}}{N(2N+2)+1} \tag{4.2}$$

where $N$ is number of nodes.

Both the bandwidth and the profile of the global stiffness matrices are significantly reduced by the using Macro-element approach, as shown in Table 4.3. A visual comparison of global stiffness matrix is shown in Figure 4.3. The reduction in the bandwidth and profile of the global stiffness matrix becomes increasingly significant, as size of the stiffness matrix increases.

### 4.2.2 Serpentine Domain with Structured Quadrilateral Mesh and Voronoi-based Mesh

In this problem, the Serpentine domain is considered with different discretizations for the traditional GSM and the Macro-element approach. This is to obtain a similar number of bars so that we may compare the final topolo-

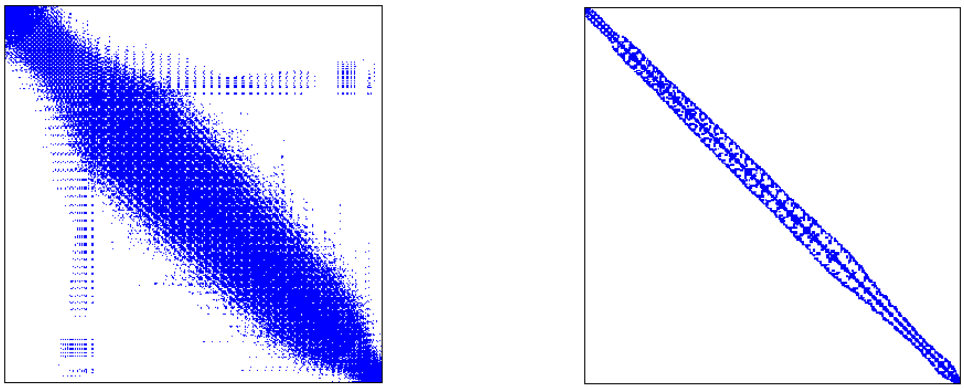

(a) (b)

Figure 4.3: Global stiffness matrix after RCM algorithm from Wrench example using: (a) traditional full level GSM; (b) Macro-element approach.

gies from each method. To show the compatibility and flexibility of the Macro-element approach with different types of discretization, two different discretizations are used, i.e. structured quadrilateral meshes and Vonoroi-based meshes. The geometry, load and support conditions of the serpentine domain are illustrated in Figure 4.4(a). The structured quadrilateral mesh was generated by ABAQUS, while the Voronoi-based mesh was generated by PolyMesher. In order to maintain a similar number of bars, meshes with different levels of refinement were used for the traditional GSM and the Macro-element approach. For a structured quadrilateral discretization, the traditional GSM used 2781 elements while the Macro-element approach used 380 elements with 5 additional nodes inserted per edge. For a Voronoi-based discretization, the traditional GSM used 550 Voronoi elements and the Macro-element approach used 250 elements with 4 nodes inserted per edge. The final topologies from the two approach are shown in Figure 4.5. The number of bars, computational cost and compliance values are summarized in Table 4.4.

Both the traditional GSM and the Macro-element approach result in similar compliance values and optimized topologies. However, the traditional

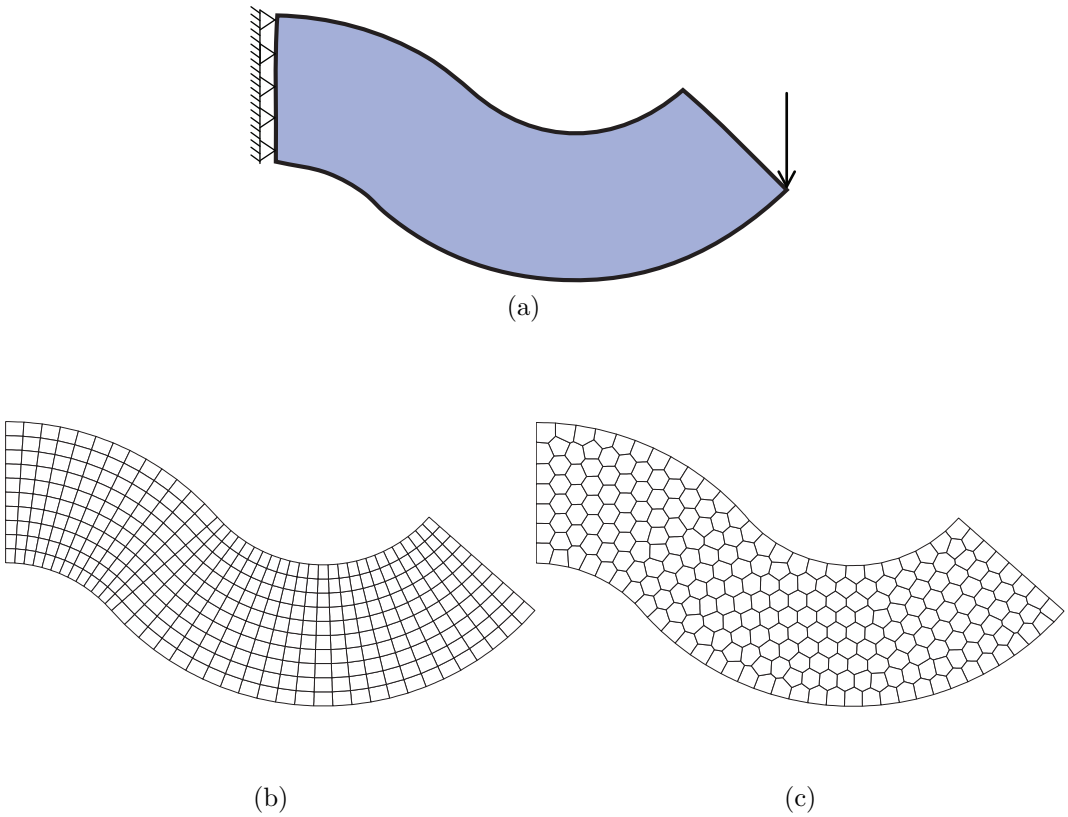

(a)

(b) (c)

Figure 4.4: Serpentine domain example with Quadrilateral mesh and Voronoi-based mesh: (a) Serpentine domain and boundary conditions; (b) quadrilateral discretization; (c) Voronoi-based discretization.

| | | Number of Bars | Compliance |
|---|---|---|---|
| Quadrilateral Mesh (Figure 4.5(a), (c)) | Traditional | 72453 | 0.589 |
| | Macro-element | 77808 | 0.585 |
| Voronoi-based Mesh (Figure 4.5(b), (d)) | Traditional | 84062 | 0.600 |
| | Macro-element | 82530 | 0.590 |

Table 4.4: Numerical information for the serpentine problem.

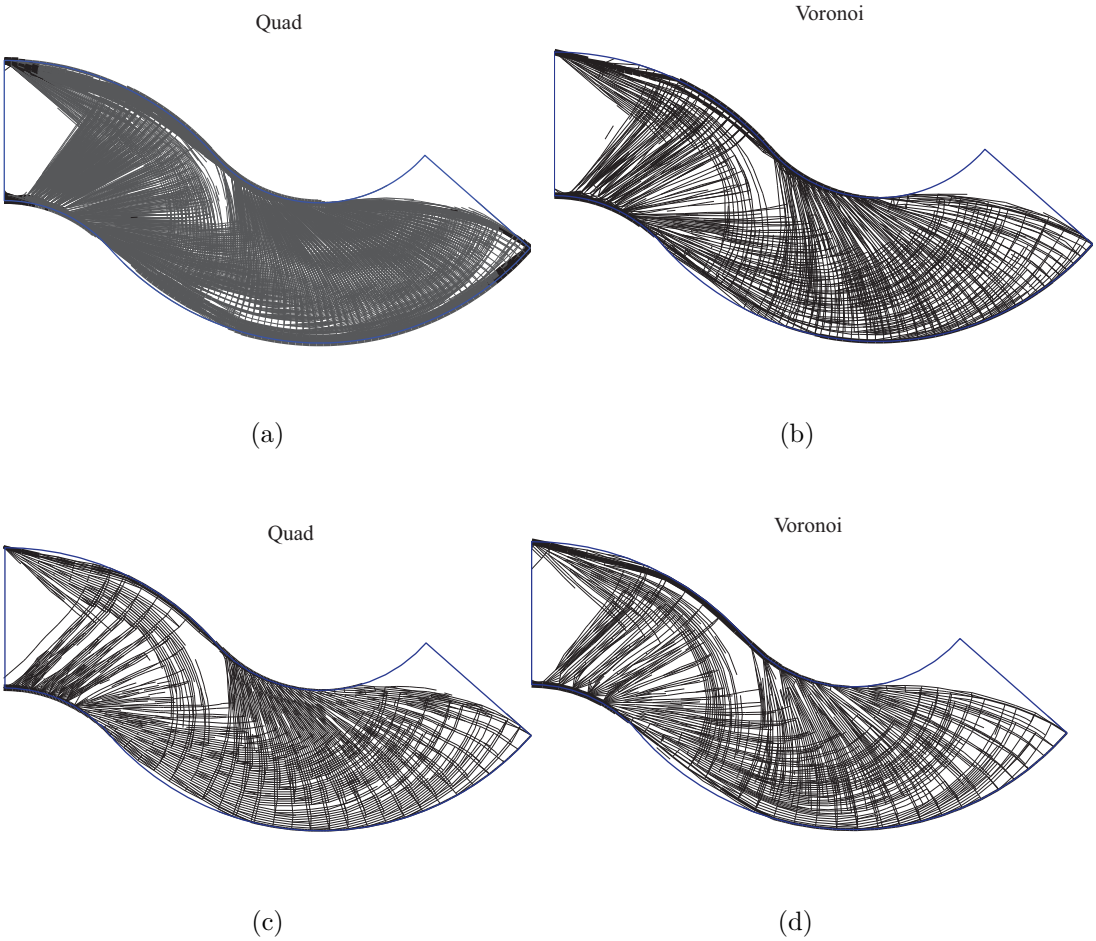


Figure 4.5: Final topologies for Serpentine domain example using classic GSM and Macro-element approach: (a) full level ground structure method using 2781 structured quadrilateral elements; (b) full level ground structure method using 1250 Voronoi-based elements; (c) the Macro-element approach using 380 structured quadrilateral elements with 5 additional nodes inserted along each edge; (d) the Macro-element approach using 250 Voronoi-based elements with 4 additional nodes inserted along each edge.

GSM requires additional boundary information to generate a valid initial ground structure and overlapping bars were involved. In the Macro-element approach, since we only connect bars within each element, there is no need to detect the boundary or search for a large number of overlapping bars because the overlapping bars were removed efficiently and systematically. This showcases the capability of the proposed method to obtain similar topologies as the traditional GSM, while offering simple and effective ground structure generation. Further, if we compare the results from a structured quadrilateral mesh and a Voronoi-based mesh, they yield almost the same truss layouts with similar topology and bar distributions. However, for complex domains such as the Serpentine domain, Voronoi-based meshes can discretize the domain with ease. Furthermore, for a coarse mesh discretization on a non-trivial domain, a Voronoi-based mesh can provide more directions for the bars to span and hence can result in a better solution when compared to results obtained using a structured quadrilateral mesh.

## 4.3 Macro-Element Approach: Comparison with Continuum Structural Optimization Solution

In this example, the final topology of the Hook problem using the GSM with the Macro-element approach is compared with a density based optimization solution using PolyTop [15], as shown in Figure 4.6. Both solutions are obtained using Voronoi-based discretizations. Qualitatively, both topologies seem to converge to the same solution and have similar traits, such as a fan feature in the center. This suggests that the GSM using the Macro-element approach can offer accurate and promising designs.

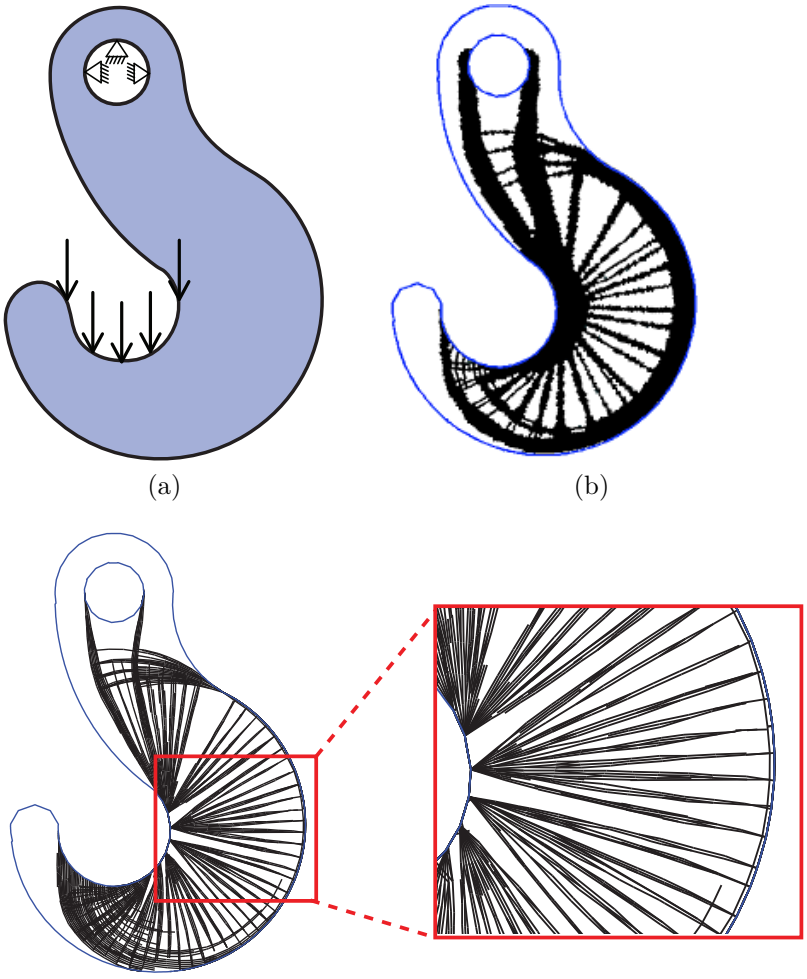

Figure 4.6: Hook domain example for continuum structural optimization and for truss optimization using GSM with the Macro-element approach: (a) domain and boundary conditions; (b) final topology from continuum optimization using PolyTop (R =2.0, v = 0.3); (c) final topology from truss optimization using the GSM with the Macro-element approach (400 Voronoi-based elements with 5 additional nodes inserted per edge).

# Chapter 5

# Conclusions

In this thesis, the generation of initial ground structures for generic 2D and 3D domains has been discussed and explored. Two types of discretization are used, structured quadrilateral discretizations and Voronoi-based discretizations. They offer alternative approaches for ground structure generation. Further, a bar generation approach has been presented: the Macro-element approach. This approach can efficiently generate an initial ground structure. It avoids invalid connections outside the boundary of concave domains, reduces the bandwidth of the global stiffness matrix, provides more control over the bar connectivity, and reduces the generation of overlapping bars. From Example 4.1, the proposed Macro-element approach is shown to yield similar numerical (discretized) results to the exact solution. In addition, the Macro-element approach converges to a similar solution to that in the traditional full-level GSM, at a lower computational cost, and offers a simple alternative way of generating initial ground structures. Example 4.2 highlights the features of the Macro-element approach for domains with complex geometries. Furthermore, the topology from the Macro-element approach in Example 4.3 shows excellent agreement with the topology obtained from continuum structural optimization. This work offers room for future extensions. They include exploring the Macro-element for 3D Voronoi tessellations and investigating the plastic formulation approach.

# Appendix A

# Sensitivity Analysis

Using the Nested formulation [3], the sensitivity of the objective function can be calculated by the adjoint method:

$$C = \boldsymbol{f}^{\mathbf{T}}\boldsymbol{u}(\boldsymbol{a}) + \boldsymbol{\lambda}^{\mathbf{T}}\left[\boldsymbol{K}(\boldsymbol{a})\boldsymbol{u}(\boldsymbol{a}) - \boldsymbol{f}\right] \tag{A.1}$$

Taking the derivative of the objective function with respect to the design variables yield the relation:

$$\frac{\partial C}{\partial a_i} = \boldsymbol{f}^{\boldsymbol{T}}\frac{\partial \boldsymbol{u}(\boldsymbol{a})}{\partial a_i} + \boldsymbol{\lambda}^{T}\left[\frac{\partial \boldsymbol{K}(\boldsymbol{a})}{\partial a_i}\boldsymbol{u}(\boldsymbol{a}) - \boldsymbol{K}(\boldsymbol{a})\frac{\partial \boldsymbol{u}(\boldsymbol{a})}{\partial a_i}\right] \tag{A.2}$$

If we assume that the equilibrium condition is satisfied implicitly, the vector $\boldsymbol{\lambda}$ can have any value. By choosing $\boldsymbol{\lambda} = -\boldsymbol{K}(\boldsymbol{a})^{-1}\boldsymbol{f} = -\boldsymbol{u}$, we can eliminate the terms in Equation (A.2) containing $\frac{\partial \boldsymbol{u}(\boldsymbol{a})}{(\partial a_i)}$. Finally, the sensitivity of the objective function has the form:

$$\frac{\partial C}{\partial a_i} = -\boldsymbol{u}^{\mathbf{T}}\frac{\partial \boldsymbol{K}(\boldsymbol{a})}{\partial a_i}\boldsymbol{u} \tag{A.3}$$

The sensitivity of the volume constraint can be calculated as:

$$\frac{\partial g}{\partial a_i} = L_i \tag{A.4}$$

# Appendix B

# Karush-Kuhn-Tucker (KKT) Conditions

Because the optimization problem in Equations (2.4) is convex, the KKT conditions are both necessary and sufficient optimality conditions. To define them, we start with the Lagrangian:

$$L(\boldsymbol{a}, \phi) = C(\boldsymbol{a}) + \phi(\sum_{i=1}^{n} a_i L_i - V_{\max}) \tag{B.1}$$

Therefore

$$\frac{\partial L}{\partial a_i}(\boldsymbol{a}^*, \phi^*) \leq 0, \quad \text{if } a_i^* = a_i^{\max} \tag{B.2}$$

$$\frac{\partial L}{\partial a_i}(\boldsymbol{a}^*, \phi^*) = 0, \quad \text{if } a_i^{\min} < a_i^* < a_i^{\max} \tag{B.3}$$

$$\frac{\partial L}{\partial a_i}(\boldsymbol{a}^*, \phi^*) \geq 0, \quad \text{if } a_i^* = a_i^{\min} \tag{B.4}$$

The derivative the Lagrangian is given as:

$$\frac{\partial L}{\partial a_i}(\boldsymbol{a}, \phi) = \frac{\partial C(\boldsymbol{a})}{\partial a_i} + \phi L_i \tag{B.5}$$

After substitution of Equation (A.3) into Equation (B.5) and, subsequently, Equations (B.2) through (B.4), we obtain the following resulting KKT conditions at the point $(\boldsymbol{a}^*, \phi^*)$:

$$\boldsymbol{u}^{\mathbf{T}} \frac{\partial \boldsymbol{K}(\boldsymbol{a})}{\partial a_i} \boldsymbol{u} \geq \phi^*, \quad \text{if } a_i^* = a_i^{\max} \tag{B.6}$$

$$\boldsymbol{u}^{\mathbf{T}} \frac{\partial \boldsymbol{K}(\boldsymbol{a})}{\partial a_i} \boldsymbol{u} = \phi^*, \quad \text{if } a_i^{\min} < a_i^* < a_i^{\max} \tag{B.7}$$

$$\boldsymbol{u}^{\mathbf{T}} \frac{\partial \boldsymbol{K}(\boldsymbol{a})}{\partial a_i} \boldsymbol{u} \leq \phi^*, \quad \text{if } a_i^* = a_i^{\min} \tag{B.8}$$

Based on Equation (B.7), we obtain constant specific strain energy at the optimum in the linear case, which corresponds to a fully stressed design with $\Psi_i = (\sigma_i^2)/E_o$, where $\Psi_i$ is the strain energy of member $i$.

# Appendix C

# Optimality Criteria (OC) Method

The optimization in this work is solved by the OC algorithm.Thus the outline of OC algorithm is presented in this Appendix. This algorithm can be derived by replacing the objective and constraints functions with the approximations on the current design point using an intermediate variable. In such way, a sequence of separable and explicit sub-problems is generated to approximate of the original problem. In this context, we linearized the objective function using exponential intermediate variables as [16]:

$$y_i = \left( \frac{a_i - a_i^{\min}}{a_i^{\max} - a_i^{\min}} \right)^{p_i} \tag{C.1}$$

$$C(\boldsymbol{a}) \cong \hat{C}(\boldsymbol{a}) = C\left(\boldsymbol{y}(\boldsymbol{a}^k)\right) + \left(\frac{\partial C}{\partial \boldsymbol{y}}\right)^T_{a=a^k} \left(\boldsymbol{y}(\boldsymbol{a}) - \boldsymbol{y}(\boldsymbol{a}^k)\right) \tag{C.2}$$

Then, after substitution of $\left(\frac{\partial C}{\partial y_i}\right)_{a=a_i^k} = \left(\frac{\partial C}{\partial a_j}\frac{\partial a_j}{\partial y_i}\right)_{a=a_i^k}$ and substitution of the Equation (C.1) in the Equation (C.2), the following equations are obtained:

$$\hat{C}(\boldsymbol{a}) = C\left(\boldsymbol{y}(\boldsymbol{a}^k)\right) + \sum_{i=1}^{n} \frac{\partial C}{\partial a_i} \mid_{a=a^k} \frac{1}{p_i}\left(a_i^k - a_i^{\min}\right)\left[\left(\frac{a_i - a_i^{\min}}{a_i^{\mathrm{k}} - a_i^{\min}}\right)^{p_i} - 1\right] \tag{C.3}$$

$$\min_{\boldsymbol{a}} \hat{C}(\boldsymbol{a})$$

$$\text{s.t.} \begin{cases} g(\boldsymbol{a}) = \boldsymbol{a}^T \mathbf{L} - V_{\max} = 0 \\ \\ a_{\min} \leq a_i \leq a_{\max} \, \forall i = 1 \, : \, M \end{cases} \tag{C.4}$$

By means of the Lagrangian duality, this problem can be solved with:

$$L(\boldsymbol{a}, \gamma) = \hat{C}(\boldsymbol{a}) + \beta \, g(\boldsymbol{a}) \tag{C.5}$$

where β is a Lagrangian multiplier and the optimality conditions are given as:

$$\frac{\partial L}{\partial a_i}(\boldsymbol{a}, \beta) = \frac{\partial \hat{C}(\boldsymbol{a})}{\partial a_i} + \beta \frac{\partial g(\boldsymbol{a})}{\partial a_i} = \frac{\partial C}{\partial a_i} \mid_{a=a^k} \left( \frac{a_i - a_i^{\min}}{a_i^k - a_i^{\min}} \right)^{p_i - 1} + \beta \, L_i = 0 \tag{C.6}$$

$$\frac{\partial L}{\partial \beta} = \boldsymbol{a}^T \mathbf{L} - V_{\max} = 0 \tag{C.7}$$

Solving the Equation (C.6) for $a_i(\beta)$ to obtain:

$$a_i(\beta) = a_i^* = a_i^{\min} + (B_i(\beta))^{\frac{1}{1-p_i}} \left( a_i^k - a_i^{\min} \right) \tag{C.8}$$

and substituting in Equation (C.7), the Lagrange multiplier β is obtained, for example, via bi-section method where $B_i$ is defined as:

$$B_i = - \frac{\frac{\partial C}{\partial a_i} \mid_{a=a^k}}{\beta \, L_i} \tag{C.9}$$

To calculate β and $a_i^*$, the box constraints need to be satisfied, and thus the next design point $a_i^{\text{new}}$ is defined as:

$$a_i^{new} = \begin{cases} a_i^+, & a_i^* \geq a_i^+ \\ a_i^-, & a_i^* \geq a_i^- \\ a_i^*, & \text{otherwise} \end{cases} \tag{C.10}$$

where the $a_i^+$ and $a_i^-$ are the bounds for the search region defined by:

$$a_i^- = \max(a_i^{min},\ a_i^k - move) \tag{C.11}$$

$$a_i^+ = \min(a_i^{\max},\ a_i^k + move) \tag{C.12}$$

in which the variable *move* is the move limit usually specified as a fraction of $a_i^{\max} - a_i^{\min}$. In the convex examples, presented in this work, a fast convergence is obtained using values for *move* larger than $a_i^{\max} - a_i^{\min}$.

The quantity $\eta = \frac{1}{1-p_i}$ is usually called a numerical damping factor and for $p_i = -1$, a reciprocal approximation is obtained. The $p_i$ values can be estimated using different approaches. In this work a two point approximation approach is used based on the work of Fadel et al. [17] and presented by Groenwold and Etman [16]. In this approach, the estimation of $p_i^{(k)}$ is:

$$p_i^{(k)} = 1 + \frac{\ln\left(\frac{\partial \mathrm{C}}{\partial \mathrm{a_i}}|_{\mathrm{a=a^{k-1}}} / \frac{\partial \mathrm{C}}{\partial \mathrm{a_i}}|_{\mathrm{a=a^{k}}}\right)}{\ln\left(a_i^{k-1}/a_i^k\right)} \tag{C.13}$$

where ln(.) is the natural logarithm. At the first step we use $p_i = -1$ and we restrict $-15 \leq p_i \leq -0.1$ for the subsequent iterations. The convergence criteria used is:

$$\max\left(\frac{|\ a_i^k - a_i^{k-1}\ |}{1 + a_i^{k-1}}\right) \leq tol \tag{C.14}$$

where *tol* is the tolerance.

# References


[1] A. G. M. Michell, "The Limits of Economy of Material in Frame-Structures," *Philosophical Magazine*, vol. 8, pp. 589–597, 1904.

[2] W. S. Dorn, R. E. Gomory, and H. J. Greenberg, "Automatic design of optimal structures," *Journal de Mecanique*, vol. 3, pp. 25–52, 1964.

[3] P. W. Christensen and A. Klarbring, *An Introduction to Structural Optimization*. Springer, 2009.

[4] M. P. Bendsø e and O. Sigmund, *Topology optimization: Theory, Methods, and Applications*. Berlin, Germany: Springer, 2003.

[5] O. Smith, "Generation of ground structures for 2D and 3D design domains," *Engineering Computations*, vol. 15, no. 4, pp. 462–500, 1998.

[6] M. T. Heath, *Scientific Ccomputing: An Introductory Survey*, 2nd ed. McGraw-Hill, 1997, vol. 363.

[7] T. Sokół, "A 99 line code for discretized Michell truss optimization written in Mathematica," *Structural and Multidisciplinary Optimization*, vol. 43, no. 2, pp. 181–190, 2010.

[8] M. Gilbert and A. Tyas, "Layout optimization of large-scale pin-jointed frames," *Engineering Computations*, vol. 20, no. 8, pp. 1044–1064, 2003.

[9] M. Ohsaki, *Optimization of Finite Dimensional Structures*. CRC Press, 2011.

[10] U. Kirsch, "Optimal Topologies of Structures," *Applied Mechanics Reviews*, vol. 42, pp. 223–239, 1989.

[11] K. Svanberg, "On local and global minima in structural optimization," in *New Directions in Optimum Structural Design*, E. Gallhager, R. H. Ragsdell, and O. C. Zienkiewicz, Eds. Chichester: John Wiley and Sons, 1984, pp. 327–341.

[12] C. Talischi, G. H. Paulino, A. Pereira, and I. F. M. Menezes, "PolyMesher: a general-purpose mesh generator for polygonal elements written in Matlab," *Structural and Multidisciplinary Optimization*, vol. 45, no. 3, pp. 309–328, Jan. 2012.

[13] C. Talischi, G. H. Paulino, A. Pereira, and I. F. M. Menezes, "Polygonal finite elements for topology optimization : A unifying paradigm," no. December 2009, pp. 671–698, 2010.

[14] E. Cuthill and J. McKee, "Reducing the Bandwidth of Sparse Symmetric Matrices," *Proceedings of the 1969 24th national conference of the ACM*, pp. 157–172, 1969.

[15] C. Talischi, G. H. Paulino, A. Pereira, and I. F. M. Menezes, "PolyTop: a Matlab implementation of a general topology optimization framework using unstructured polygonal finite element meshes," *Structural and Multidisciplinary Optimization*, vol. 45, no. 3, pp. 329–357, Jan. 2012.

[16] A. A. Groenwold and L. F. P. Etman, "On the equivalence of optimality criterion and sequential approximate optimization methods in the classical topology layout problem," *International Journal for Numerical Methods in Engineering*, no. May 2007, pp. 297–316, 2008.

[17] G. M. Fadel, M. F. Riley, and B. J. M, "Two point exponential approximation method for structural optimization," *Structural Optimization*, vol. 124, no. 2, pp. 117–124, 1990.

[18] W. Achtziger, "On simultaneous optimization of truss geometry and topology," *Structural and Multidisciplinary Optimization*, vol. 33, no. 4-5, pp. 285–304, Jan. 2007.

[19] W. Achtziger and M. Stolpe, "Global optimization of truss topology with discrete bar areas – Part II: Implementation and numerical results," *Computational Optimization and Applications*, vol. 44, no. 2, pp. 315–341, Dec. 2009.

[20] W. Achtziger and M. Stolpe, "Truss topology optimization with discrete design variables – Guaranteed global optimality and benchmark examples," *Structural and Multidisciplinary Optimization*, vol. 34, pp. 1–20, 2007.

[21] A. Klarbring and N. Strömberg, "A note on the min-max formulation of stiffness optimization including non-zero prescribed displacements," *Structural and Multidisciplinary Optimization*, vol. 45, no. 1, pp. 147–149, June 2011.

[22] T. Hagishita and M. Ohsaki, "Topology optimization of trusses by growing ground structure method," *Structural and Multidisciplinary Optimization*, vol. 37, no. 4, pp. 377–393, Apr. 2008.

[23] M. Ohsaki and N. Katoh, "Topology optimization of trusses with stress and local constraints on nodal stability and member intersection," *Structural and Multidisciplinary Optimization*, vol. 29, no. 3, pp. 190–197, Oct. 2004.

[24] M. Hagishita, T. Ohsaki, "Topology optimization of trusses by growing ground structure method," *Structural and Multidisciplinary Optimization*, pp. 377–393, 2009.

[25] G. I. N. Rozvany, *Structural Design via Optimality Criteriahe: Prager Approach to Structural Optimization*. Springer, 1989.

[26] G. I. N. Rozvany, "Exact analytical solutions for some popular benchmark problems in topology optimization," *Structural Optimization*, vol. 15, pp. 42–48, 1998.

[27] G. I. N. Rozvany and T. Sokół, "Exact truss topology optimization: allowance for support costs and different permissible stresses in tension and compression-extensions of a classical solution by Michell," *Structural and Multidisciplinary Optimization*, vol. 45, no. 3, pp. 367–376, Nov. 2011.

[28] O. Smith, "Topology optimization of trusses with local stability constraints and multiple loading conditions – a heuristic approach," *Structural optimization*, vol. 13, pp. 155–166, 1997.

[29] T. Sokół and G. I. N. Rozvany, "New analytical benchmarks for topology optimization and their implications. Part I: bi-symmetric trusses with two point loads between supports," *Structural and Multidisciplinary Optimization*, vol. 46, no. 4, pp. 477–486, Mar. 2012.

[30] T. Sokół and G. I. N. Rozvany, "Exact least-volume trusses for two symmetric point loads and unequal permissible stresses in tension and compression," *Structural and Multidisciplinary Optimization*, vol. 47, no. 1, pp. 151–155, Dec. 2012.

[31] K. Svanberg, "On the convexity and concavity of compliances," *Structural and Multidisciplinary Optimization*, vol. 7, pp. 42–46, 1994.